Intrinsic and extrinsic performance limits of graphene devices on SiO_2

JIAN-HAO CHEN[1,2,3], CHAUN JANG[2,3], SHUDONG XIAO[2,3], MASA ISHIGAMI[2,3†] AND MICHAEL S. FUHRER[1,2,3*]

[1]Materials Research Science and Engineering Center, University of Maryland, College Park, Maryland 20742, USA
[2]Department of Physics, University of Maryland, College Park, Maryland 20742, USA
[3]Center for Nanophysics and Advanced Materials, University of Maryland, College Park, Maryland 20742, USA
[†]Present address: Department of Physics, University of Central Florida, 4000 Central Florida Boulevard, Orlando, Florida 32816-2385, USA
*e-mail: mfuhrer@umd.edu

Published online: 23 March 2008; doi:10.1038/nnano.2008.58

The linear dispersion relation in graphene[1,2] gives rise to a surprising prediction: the resistivity due to isotropic scatterers, such as white-noise disorder[3] or phonons[4–8], is independent of carrier density, *n*. Here we show that electron–acoustic phonon scattering[4–6] is indeed independent of *n*, and contributes only 30 Ω to graphene's room-temperature resistivity. At a technologically relevant carrier density of 1×10^{12} cm^{-2}, we infer a mean free path for electron–acoustic phonon scattering of >2 μm and an intrinsic mobility limit of 2×10^5 cm^2 V^{-1} s^{-1}. If realized, this mobility would exceed that of InSb, the inorganic semiconductor with the highest known mobility ($\sim 7.7 \times 10^4$ cm^2 V^{-1} s^{-1}; ref. 9) and that of semiconducting carbon nanotubes ($\sim 1 \times 10^5$ cm^2 V^{-1} s^{-1}; ref. 10). A strongly temperature-dependent resistivity contribution is observed above ~200 K (ref. 8); its magnitude, temperature dependence and carrier-density dependence are consistent with extrinsic scattering by surface phonons at the SiO_2 substrate[11,12] and limit the room-temperature mobility to $\sim 4 \times 10^4$ cm^2 V^{-1} s^{-1}, indicating the importance of substrate choice for graphene devices[13].

The nature of electron–phonon scattering in graphene has been determined by measuring the four-probe resistivity $\rho(V_g, T)$ of graphene field-effect devices on SiO_2/Si (refs 2 and 14) versus temperature T in the range 16–485 K, with the gate voltage V_g applied to the Si substrate (see Methods). Measurements were performed in ultrahigh vacuum (UHV) on cleaned samples to minimize temperature-dependent effects due to molecular adsorption/desorption[14,15].

The dependence of resistivity on carrier density was investigated by using the gate voltage to tune the carrier density $n = c_g V_g/e$, where $c_g = 1.15 \times 10^{-8}$ F cm^{-2} is the gate capacitance and e the elementary charge. Figure 1a,b shows $\rho(V_g, T)$ for two samples at seven different gate voltages plotted on a linear scale. The $\rho(V_g, T)$ curves are linear in temperature at low T with a slope of $(4.0 \pm 0.5) \times 10^{-6} h/e^2$ K as indicated by the dashed lines. The slope is independent of carrier density, and is the same for both samples.

Longitudinal acoustic (LA) phonon scattering is expected[4–6,16] to give rise to a linear resistivity independent of carrier density:

$$\rho(V_g, T) = \rho_0(V_g) + \rho_A(T); \quad \rho_A(T) = \left(\frac{h}{e^2}\right)\frac{\pi^2 D_A^2 k_B T}{2h^2 \rho_s v_s^2 v_F^2}, \qquad (1)$$

where $\rho_0(V_g)$ is the residual resistivity at low temperature, $\rho_A(T)$ is the resistivity due to acoustic phonon scattering, k_B is the Boltzmann constant, $\rho_s = 7.6 \times 10^{-7}$ kg m^{-2} is the two-dimensional mass density of graphene, $v_F = 1 \times 10^6$ m s^{-1} is the Fermi velocity, v_s is the velocity of sound and D_A the acoustic deformation potential. For LA phonons, $v_s = 2.1 \times 10^4$ m s^{-1}, and our experimentally determined slope gives $D_A = 18 \pm 1$ eV, in good agreement with theoretical[6,16–19] and experimental[20,21] expectations. Well below the Bloch–Grüneisen temperature, $T \ll T_{BG} \approx (v_s/v_F)T_F$, where T_F is the Fermi temperature, a crossover to $\rho_A(T) \propto T^4$ is expected[6]; $T_{BG} \approx (8\text{ K})V_g^{1/2}$, where V_g is measured in volts. However, numerical calculations[6] show that $\rho(T)$ is indistinguishable from linear for temperatures above ~20 K even for $V_g = 70$ V, consistent with our measurements. (This is analogous to the familiar result for metals, where the linear temperature-dependent resistivity persists down to temperatures a small fraction of the Debye temperature.)

In contrast to the low-T behaviour, the resistivity at higher T is highly nonlinear in T, and becomes significantly dependent on V_g, increasing for decreasing V_g. Others[8] have noted the nonlinear dependence on T, but were unable to separate the low-T LA phonon contribution from the high-T contribution, nor could they identify the specific dependences on T or V_g for each contribution. The strong (activated) temperature dependence suggests scattering by a high-energy phonon mode or modes. We find that the data can be fitted by adding an extra term $\rho_B(V_g, T)$ representing the activated contribution to the resistivity:

$$\rho(V_g, T) = \rho_0(V_g) + \rho_A(T) + \rho_B(V_g, T);$$
$$\rho_B(V_g, T) = B_1 V_g^{-\alpha_1}\left(\frac{1}{e^{(59\text{meV})/k_B T} - 1} + \frac{6.5}{e^{(155\text{meV})/k_B T} - 1}\right) \qquad (2a)$$

or

$$\rho(V_g, T) = \rho_0(V_g) + \rho_A(T) + \rho_B(V_g, T);$$
$$\rho_B(V_g, T) = B_2 V_g^{-\alpha_2}\left(\frac{1}{e^{E_0/k_B T} - 1}\right). \qquad (2b)$$

For equation (2a), the particular form of the expression in parentheses in $\rho_B(V_g, T)$ is chosen to match surface phonons in SiO_2 (refs 12 and

© 2008 Nature Publishing Group

22); however, a single Bose–Einstein distribution as shown in equation (2b) can also give a reasonable fit. Figure 1c,d shows a global fit to equation (2a) (solid lines) and to equation (2b) (dashed lines) for the data for two samples. In addition to the low-temperature resistivity ρ_0, and the linear term determined above, only two additional global parameters in equation (2a) ($B_1 = 0.607(h/e^2)V^{\alpha_1}$ and $\alpha_1 = 1.04$) and three global parameters in equation (2b) ($B_2 = 3.26(h/e^2)V^{\alpha_2}$, $\alpha_2 = 1.02$, and $E_0 = 104$ meV) are used to fit the seven curves each for two devices.

We now discuss the possible origins of the activated resistivity term $\rho_B(V_g, T)$. Scattering in graphene requires a phonon wavevector $q \approx 0$ (intravalley scattering) or $q \approx \mathbf{K}$ (intervalley scattering). The next lowest-energy modes after the $q \approx 0$ acoustic modes are the zone boundary ZA phonon ($q = \mathbf{K}$) at $\hbar\omega \approx 70$ meV and the optical ZO mode ($q = 0$) at $\hbar\omega \approx 110$ meV (ref. 23). The optical ZO mode is consistent with the observed temperature dependence according to the fit to equation (2b). However, both modes are out-of-plane vibrations, which are not expected to couple strongly to the electrons[17–20]; for example, scattering by these modes is not observed in carbon nanotubes, but scattering by the longitudinal zone-boundary phonon with $\hbar\omega \approx 160$ meV is extremely strong[24] (but our data are poorly fit to a Bose–Einstein distribution with $\hbar\omega \approx 160$ meV). The strong carrier density dependence $\rho_B(V_g, T) \propto V_g^{-1.04}$ is also inconsistent with graphene optical phonon scattering, which should depend very weakly on carrier density[6]. Breaking of the inversion symmetry of the graphene sheet by the substrate induces an additional perturbation potential for the out-of-plane phonon modes, but reasonable estimates of the size of this perturbation are too small to account for the observed $\rho_B(V_g, T)$. Thus we reject optical phonon modes of graphene as the source of $\rho_B(V_g, T)$.

Another possible origin of $\rho_B(V_g, T)$ is remote interfacial phonon (RIP) scattering[11] by the polar optical phonons of the SiO_2 substrate. Recently, this has been discussed theoretically in the context of graphene[12]. The two strongest surface optical phonon modes in SiO_2 are calculated to have $\hbar\omega \approx 59$ meV and 155 meV, with a ratio of coupling to the electrons of 1:6.5 (refs 12 and 22); we used these parameters as inputs to equation (2a), and the fit shows that they reasonably describe the temperature dependence of $\rho_B(V_g, T)$ (Fig. 1c,d). The magnitude of the RIP scattering resistivity predicted by Fratini and Guinea[12] is on the order of a few $10^{-3}h/e^2$ at 300 K, also in agreement with the observed magnitude. RIP results in a long-range potential, which gives rise to a density-dependent resistivity in graphene, similar to charged impurity scattering. Specifically, in the simplest case, the electron–phonon matrix $|H_{\mathbf{kk'}}|^2$ element is proportional to q^{-1}, where q is the scattering wavevector, and the resistivity is proportional to $k_F^{-1} \propto V_g^{-1/2}$. However, finite-$q$ corrections to $|H_{\mathbf{kk'}}|^2$ lead to a stronger dependence of $\rho_B(V_g, T)$ on V_g (ref. 12), so the observed $\rho_B(V_g, T) \propto V_g^{-1.04}$ is also reasonable. RIP scattering by the polar optical phonons of the SiO_2 substrate therefore naturally explains the magnitude, temperature dependence, and charge carrier density dependence of $\rho_B(V_g, T)$; hence we consider RIP scattering to be the most likely origin of $\rho_B(V_g, T)$.

Finally, we note that although our measurements were performed on clean samples in UHV, the temperature-dependent component of the resistivity is consistent in magnitude with earlier, more limited studies of $\rho(V_g, T)$ in graphene[7,8], where resist residue and adsorbed atmospheric species were not rigorously controlled (although the residual resistivity shows larger variations). This supports our conclusion that the observed temperature-dependent resistivity is intrinsic to the graphene/SiO_2 system. We also note that graphene on SiC should have significantly reduced RIP scattering[12]; this is supported by an estimate of the electron–phonon scattering time for graphene on SiC at $T = 300$ K of $\sim 4 \times 10^{-12}$ s at $n = 3.4 \times 10^{12}$ cm^{-2} (ref. 25), compared to $\sim 0.6 \times 10^{-12}$ s at the same carrier density in our samples.

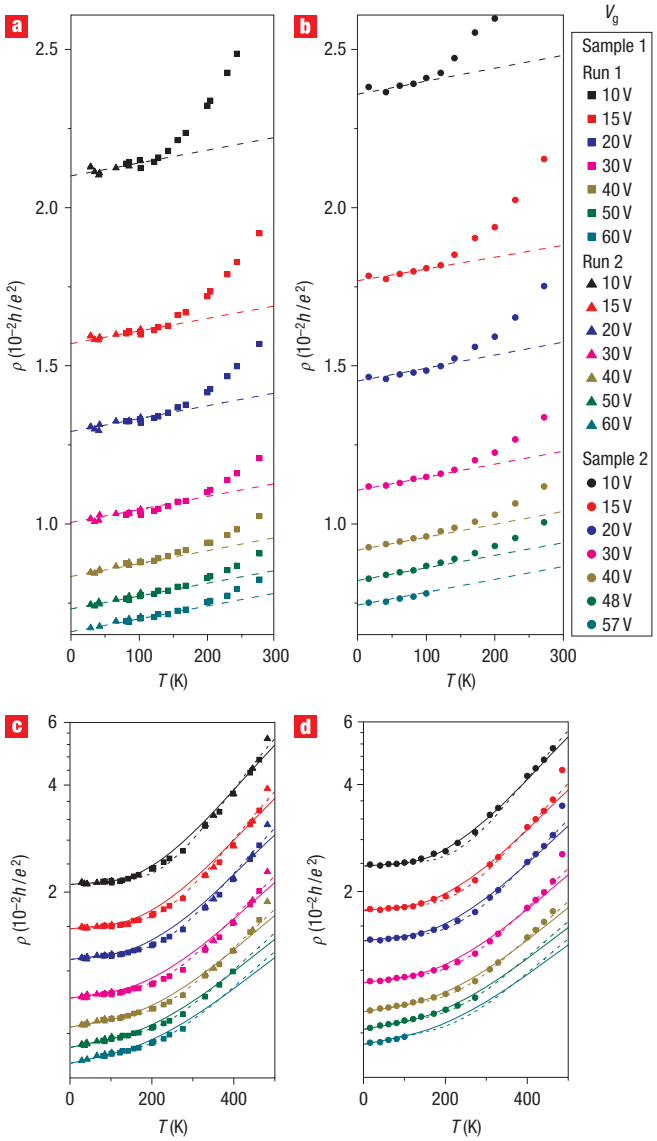

Figure 1 Temperature-dependent resistivity of graphene on SiO_2. **a**,**b**, Resistivity of two graphene samples (sample 1, **a**; sample 2, **b**) as a function of temperature for gate voltages from 10 to 60 V. Dashed lines are fits to the linear T-dependence (equation (1)). **c**,**d**, Same data as in **a**,**b** on a logarithmic scale. The solid lines are fits to equation (2a) (acoustic phonon scattering in graphene plus optical phonon scattering due to the SiO_2 substrate) and the dashed lines are fits to equation (2b) (the same acoustic phonon scattering term plus a single Bose–Einstein term).

The contributions of the acoustic phonons and remote interfacial phonons can be used to determine the room-temperature intrinsic limits to the resistivity and mobility in graphene, and extrinsic limits for graphene on SiO_2. Figure 2a shows the gate voltage dependence of the three components of the resistivity (ρ_0, ρ_A and ρ_B) corresponding to scattering by impurities, graphene LA phonons and RIP scattering by SiO_2

© 2008 Nature Publishing Group

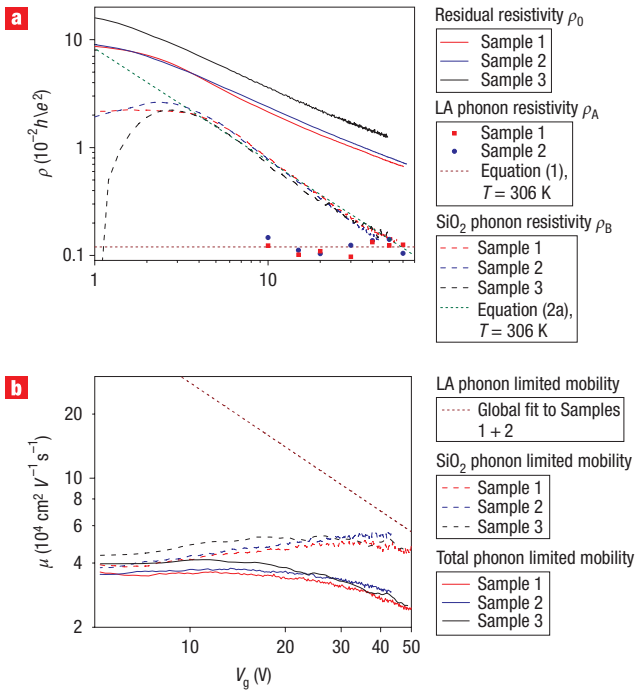

Figure 2 Room-temperature performance limits of graphene on SiO_2. **a**, Residual resistivity ρ_0, acoustic phonon resistivity ρ_A and SiO_2 remote interfacial phonon resistivity ρ_B as a function of gate voltage near room temperature for three samples. **b**, Gate-voltage-dependent mobility limits at room temperature corresponding to scattering by acoustic phonons (short-dashed line), SiO_2 surface phonons (long-dashed lines) and both phonon contributions (solid lines).

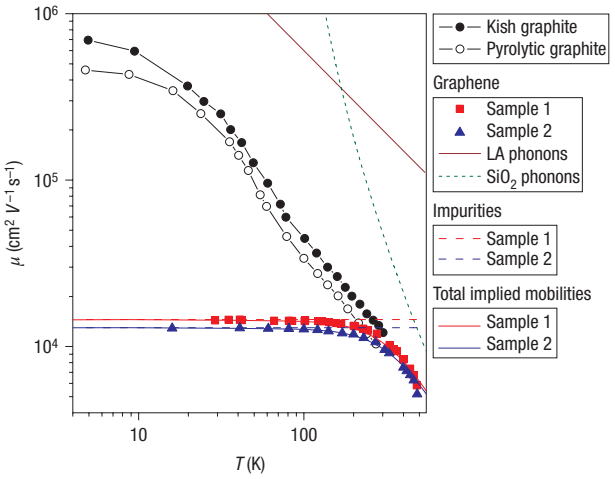

Figure 3 Temperature dependence of mobility in graphene and graphite. The temperature-dependent mobilities of graphene sample 1 (red squares) and sample 2 (blue triangles) at $V_g = 14$ V ($n = 1 \times 10^{12}$ cm^{-2}) are compared with Kish graphite (filled black circles) and pyrolytic graphite (open black circles)[27]. The mobility limits in graphene determined in this work for scattering by LA phonons (dark red solid line), remote interfacial phonon scattering (green dashed line), and impurity scattering (red and blue dashed lines) are shown. Red and blue solid lines show the expected net mobility for each sample, according to Matthiessen's rule.

phonons, respectively, near room temperature for three different graphene samples. ($T = 330$ K, 308 K and 306 K for samples 1, 2 and 3, respectively; sample 1 and sample 2 are the same samples as shown in Fig. 1, and sample 3 is a lower mobility sample for which we have limited temperature dependence data.) The residual impurity resistivity $\rho_0(V_g)$ (solid lines) is estimated, with an error not greater than 1.5%, by taking $\rho(V_g, T)$ at low temperature ($T = 29$ K, 16 K and 20 K for samples 1, 2 and 3, respectively). The graphene LA phonon resistivity ρ_A (306 K) $= 1.2 \times 10^{-3} h/e^2$ (dark red dashed line) is obtained from the global fit to equation (1) for samples 1 and 2; the solid symbols are obtained from individual fits to $\rho(T)$ at various V_g. The RIP scattering resistivity $\rho_B(V_g, T \approx$ room temperature) (long-dashed lines) is obtained by subtracting $\rho_A(T)$ and $\rho_0(V_g)$ from $\rho(V_g, T)$ for each sample. Although $\rho_0(V_g)$ varies by a factor of 1.7 among the three samples, the temperature-dependent resistivities $\rho_B(V_g, T)$ are nearly equal except very close to the MCP (see Supplementary Information); this verifies that the temperature-dependent resistivity terms ρ_A and ρ_B arise from phonon scattering, which is disorder-independent. The power-law behaviour of the activated contribution $\rho_B(V_g, 306\text{ K}) \propto V_g^{-1.04}$ can also clearly be seen.

Figure 2b shows the corresponding room-temperature mobility $\mu = 1/ne\rho = 1/c_g V_g \rho$ calculated for each phonon resistivity contribution in Fig. 2a as a function of gate voltage. If the properties of graphene were limited by the intrinsic LA phonon scattering as the dominant intrinsic source of resistivity, the room-temperature intrinsic resistivity of graphene would be 30 Ω, independent of carrier density, and the mobility would diverge at low carrier density as n^{-1}. At a technologically relevant carrier density of $n = 1 \times 10^{12}$ cm^{-2} ($V_g = 14$ V), the intrinsic mobility would then be 2×10^5 cm^2 V^{-1} s^{-1}, higher than any known semiconductor. If the only extrinsic limit to the mobility of graphene on SiO_2 were due to RIP scattering, graphene on SiO_2 would still have a room-temperature mobility of 4×10^4 cm^2 V^{-1} s^{-1}, which compares favourably with the best InAs and InSb field-effect transistors (FETs) (ref. 26). The dominance of RIP scattering over LA phonon scattering at room temperature poses an interesting trade-off; high-κ dielectrics may be used to reduce the scattering contribution from defects (that is, ρ_0) due to increased screening of the impurity potential, but will increase scattering due to RIP (ref. 12).

Figure 3 shows the temperature dependence of the mobility of sample 1 and sample 2 at $n = 1 \times 10^{12}$ cm^{-2} ($V_g = 14$ V), as well as the limits due to scattering by LA phonons, polar optical phonons of the SiO_2 substrate, and impurities. As shown in Fig. 3, even for the cleanest graphene devices fabricated to date, impurity scattering is still the dominant factor limiting the mobility for $T < 400$ K. For comparison, the temperature-dependent mobility in Kish graphite and pyrolytic graphite from ref. 27 are also shown; these are the two materials commonly used as sources for exfoliated graphene on SiO_2. The significantly higher mobility at low temperature in Kish and pyrolytic graphites compared to graphene is a strong indication that the impurity scattering in graphene on SiO_2 is not due to point defects present in the parent material, but rather is likely caused by charged impurities in the SiO_2 substrate[14,28]. It is important to note that the closeness of the room-temperature mobility values for graphene and bulk graphite is a coincidence, and removing impurity scattering in graphene will greatly increase not only the low-temperature mobility, but the room-temperature mobility as well.

Our data give a complete picture of the current limitations and future promise of graphene as an electronic material. Currently, the mobility of graphene on SiO_2 at low and room temperatures is limited by impurity scattering, likely due to charged impurities in

© 2008 Nature Publishing Group

the SiO_2 substrate[14,28]. If charged impurity scattering can be reduced, the room-temperature mobility, limited by extrinsic RIP scattering due to SiO_2 phonons, could be improved to 4×10^4 cm^2 V^{-1} s^{-1}, comparable to the best FETs[26]. With proper choice of substrate[13,25], or by suspending graphene, the intrinsic limit of mobility of 2×10^5 cm^2 V^{-1} s^{-1} at room temperature could be realized. This would dramatically enhance the application of graphene field-effect devices to chemical sensing, high-speed analogue electronics, and spintronics. In addition, ballistic transport over micrometre lengths would open the possibility of new electronic devices based on quantum transport operating at room temperature.

Note added in proof: After this manuscript was submitted, we became aware of the note added in the published version of ref. 8, which points out that graphene on poly(methylmethacrylate) (PMMA) (studied in ref. 8) shows a similar rise in resistivity (at least up to room temperature) as graphene on SiO_2, and takes this as evidence that RIP scattering is unlikely to be the source of the upturn. It is difficult to make any quantitative comparison of our data with those of ref. 8, because their model and analysis specifically exclude any carrier density dependence of the resistivity upturn, contrary to the experimental observation. However, it is quite plausible that PMMA shows similar RIP scattering to SiO_2 because (1) contrary to the claim of ref. 8, PMMA and SiO_2 have almost identical low- and high-frequency dielectric constants, and (2) PMMA shows a number of infrared-active phonon modes in the range 60–120 meV (as well as higher energies; see, for example, the Spectral Database for Organic Compounds, AIST, Japan) which could give rise to a resistivity upturn at room temperature.

METHODS

Graphene was obtained from Kish graphite by mechanical exfoliation[2] on 300-nm SiO_2 over doped Si (back gate), with Au/Cr electrodes defined by electron-beam lithography. Raman spectroscopy confirmed that the samples were single-layer graphene[14,29] (see Supplementary Information for device pictures and Raman spectra). After fabrication, the devices were annealed in H_2/Ar at 300 °C for 1 h to remove resist residues[14,30].

In order to eliminate possible effects on the resistivity due to temperature-dependent concentrations of adsorbates on the graphene[14,15], all measurements were performed in UHV. The devices were mounted on a liquid helium cooled cold finger in a UHV chamber, allowing temperature control between 16 K and 490 K. Following a vacuum chamber bakeout, each device was annealed in UHV at 490 K overnight to remove residual adsorbed gases. Experiments were carried out at pressure lower than 2×10^{-9} torr at 490 K and 1×10^{-10} torr below 300 K. The device temperature was tuned from 485 K to room temperature using a heater installed on the cold finger, and controlled liquid helium flow was used to tune the device temperature from 290 K to 16 K, with resistivity versus gate voltage $\rho(V_g)$ curves taken at various temperature points. Warming experiments were also performed, where the device temperature was raised from 16 K to 243 K by controlling the helium flow. Heater operation was avoided at low temperature to prevent outgassing of the cold finger. Transport properties of the samples between cooling and warming were very reproducible, showing no detectable effect of residual gas absorbed on the samples during the experiment; the exception is that small differences in cooling and warming data were occasionally observed very near the minimum conductivity point (MCP) (see Supplementary Information).

Resistivity measurements were performed using a standard four-probe technique and error in determining the aspect ratio (and hence the absolute magnitude of the resistivity) was estimated to be 10% (ref. 14). Resistivity versus gate voltage $\sigma(V_g)$ curves were shifted by a constant threshold voltage V_{th} in order to define $V_g = 0$ as the MCP. V_{th} is small ($V_{th} = 0$ V for sample 1 and -3 V for sample 2) and does not change with temperature for cleaned samples that are outgassed sufficiently in UHV. Sample 3 was prepared in the same way as Sample 1 and Sample 2, and then multiple potassium deposition and removal cycles were carried out in UHV, resulting in an increased density of immobile impurities and lowered mobility[14]. ($V_{th} = -8.2$ V for sample 3.)

Received 6 December 2007; accepted 19 February 2008; published 23 March 2008.

References

1. Novoselov, K. S. *et al.* Electric field effect in atomically thin carbon films. *Science* **306,** 666–669 (2004).
2. Novoselov, K. S. *et al.* Two-dimensional atomic crystals. *Proc. Natl Acad. Sci. USA* **102,** 10451–10453 (2005).
3. Shon, N. H. & Ando, T. Quantum transport in two-dimensional graphite system. *J. Phys. Soc. Jpn* **67,** 2421–2429 (1998).
4. Pietronero, L., Strässler, S., Zeller, H. R. & Rice, M. J. Electrical conductivity of a graphite layer. *Phys. Rev. B* **22,** 904–910 (1980).
5. Stauber, T., Peres, N. M. R. & Guinea, F. Electronic transport in graphene: A semi-classical approach including midgap states. *Phys. Rev. B* **76,** 205423 (2007).
6. Hwang, E. H. & Sarma, S. D. Acoustic phonon scattering limited carrier mobility in 2D extrinsic graphene. http://arxiv.org/abs/0711.0754 (2007).
7. Tan, Y.-W., Zhang, Y., Stormer, H. L. & Kim, P. Temperature dependent electron transport in graphene. *Eur. Phys. J. Special Topics* **148,** 15–18 (2007).
8. Morozov, S. V. *et al.* Giant intrinsic carrier mobilities in graphene and its bilayer. *Phys. Rev. Lett.* **100,** 016602 (2008).
9. Hrostowski, H. J., Morin, F. J., Geballe, T. H. & Wheatley, G. H. Hall effect and conductivity of InSb. *Phys. Rev.* **100,** 1672–1676 (1955).
10. Dürkop, T., Getty, S. A., Cobas, E. & Fuhrer, M. S. Extraordinary mobility in semiconducting carbon nanotubes. *Nano Lett.* **4,** 35–39 (2004).
11. Hess, K. & Vogl, P. Remote polar scattering in silicon inversion layers. *Solid State Commun.* **30,** 807–809 (1979).
12. Fratini, S. & Guinea, F. Substrate limited electron dynamics in graphene. http://arxiv.org/abs/0711.1303 (2007).
13. Chen, J. H. *et al.* Printed graphene circuits. *Adv. Mater.* **19,** 3623–3627 (2007).
14. Chen, J. H. *et al.* Charged impurity scattering in graphene. *Nature Phys.* (in press). http://arxiv.org/abs/0708.2408.
15. Schedin, F. *et al.* Detection of individual gas molecules adsorbed on graphene. *Nature Mater.* **6,** 652–655 (2007).
16. Woods, L. M. & Mahan, G. D. Electron–phonon effects in graphene and armchair (10,10) single-wall carbon nanotubes. *Phys. Rev. B* **61,** 10651–10663 (2000).
17. Suzuura, H. & Ando, T. Phonons and electron–phonon scattering in carbon nanotubes. *Phys. Rev. B* **65,** 235412 (2002).
18. Pennington, G. & Goldsman, N. Semiclassical transport and phonon scattering of electrons in semiconducting carbon nanotubes. *Phys. Rev. B* **68,** 045426 (2003).
19. Perebeinos, V., Tersoff, J. & Avouris, P. Electron–phonon interaction and transport in semiconducting carbon nanotubes. *Phys. Rev. Lett.* **94,** 086802 (2005).
20. Ono, S. & Sugihara, K. Theory of the transport properties in graphite. *J. Phys. Soc. Jpn* **21,** 861–868 (1966).
21. Zhou, X., Park, J.-Y., Huang, S., Liu, J. & McEuen, P. L. Band structure, phonon scattering, and the performance limit of single-walled carbon nanotube transistors. *Phys. Rev. Lett.* **95,** 146805 (2005).
22. Fischetti, M. V., Neumayer, D. A. & Cartier, E. A. Effective electron mobility in Si inversion layers in metal-oxide-semiconductor systems with high-k insulator: The role of remote phonon scattering. *J. Appl. Phys.* **90,** 4587–4608 (2001).
23. Mohr, M. *et al.* Phonon dispersion of graphite by inelastic x-ray scattering. *Phys. Rev. B* **76,** 035439 (2007).
24. Yao, Z., Kane, C. L. & Dekker, C. High-field electrical transport in single-wall carbon nanotubes. *Phys. Rev. Lett.* **84,** 2941–2944 (2000).
25. Berger, C. *et al.* Electronic confinement and coherence in patterned epitaxial graphene. *Science* **312,** 1191–1196 (2006).
26. Bennett, B. R., Magno, R., Boos, J. B., Kruppa, W. & Ancona, M. G. Antimonide-based compound semiconductors for electronic devices: A review. *Solid State Electron.* **49,** 1875–1895 (2005).
27. Sugihara, K., Kawamura, K. & Tsuzuku, T. Temperature dependence of the average mobility in graphite. *J. Phys. Soc. Jpn* **47,** 1210–1215 (1979).
28. Adam, S., Hwang, E. H., Galitski, V. M. & Sarma, S. D. A self-consistent theory for graphene transport. *Proc. Natl Acad. Sci. USA* **104,** 18392–18397 (2007).
29. Ferrari, A. C. *et al.* Raman spectrum of graphene and graphene layers. *Phys. Rev. Lett.* **97,** 187401 (2006).
30. Ishigami, M., Chen, J. H., Cullen, W. G., Fuhrer, M. S. & Williams, E. D. Atomic structure of graphene on SiO_2. *Nano Lett.* **7,** 1643–1648 (2007).

Acknowledgements

We acknowledge stimulating discussions with S. Das Sarma, E. Hwang, S. Adam, S. Fratini and E. D. Williams. We also thank E. D. Williams for use of UHV facilities. This work has been supported by the U.S. Office of Naval Research grant no. N000140610882 (CJ, SX, MSF), National Science Foundation grant no. CCF-06-34321 (MSF), and the NSF-UMD-MRSEC grant no. DMR 05-20471 (JHC). M.I. is supported by the Intelligence Community Postdoctoral Fellowship programme.
Correspondence and requests for materials should be addressed to M.S.F.
Supplementary Information accompanies this paper at www.nature.com/naturenanotechnology.

Author contributions

M.S.F. and M.I. conceived the experiments, M.I. designed the experimental apparatus, J.H.C. performed the bulk of the experiments and data analysis, C.J. and S.X. fabricated devices and aided in the experiments, and M.S.F. and J.H.C. co-wrote the paper. All authors discussed the results and commented on the manuscript.

Reprints and permission information is available online at http://npg.nature.com/reprintsandpermissions/

© 2008 Nature Publishing Group